



CHORUS

This is the accepted manuscript made available via CHORUS. The article has been published as:

Thickness-tuned transition of band topology in ZrTe₅ nanosheets

Jianwei Lu, Guolin Zheng, Xiangde Zhu, Wei Ning, Hongwei Zhang, Jiyong Yang, Haifeng Du, Kun Yang, Haizhou Lu, Yuheng Zhang, and Mingliang Tian

Phys. Rev. B **95**, 125135 — Published 29 March 2017

DOI: [10.1103/PhysRevB.95.125135](https://doi.org/10.1103/PhysRevB.95.125135)

Thickness-tuned transition of band topology in ZrTe₅ nanosheets

Jianwei Lu,^{1,2*} Guolin Zheng,^{1,2*} Xiangde Zhu,¹ Wei Ning,^{1,3,†} Hongwei Zhang,^{1,2} Jiyong Yang,¹
Haifeng Du,^{1,3} Kun Yang,⁴ Haizhou Lu,⁵ Yuheng Zhang,^{1,2,3} and Mingliang Tian^{1,2,3†}

¹High Magnetic Field Laboratory, Chinese Academy of Sciences, Hefei 230031, Anhui, China

²Department of physics, University of Science and Technology of China, Hefei 230026, China

³Collaborative Innovation Center of Advanced Microstructures, Nanjing University, Nanjing 210093, China

⁴National High Magnetic Field Laboratory, Florida State University, Tallahassee, Florida 32306-4005, USA

⁵Department of Physics, South University of Science and Technology of China, Shenzhen 518055, China

*Those authors contribute equally to this work

†To whom correspondence should be addressed. E-mails: ningwei@hmfl.ac.cn; tianml@hmfl.ac.cn

Abstract

We report thickness-tuned electrical transport in highly anisotropic three-dimensional Dirac semimetal ZrTe_5 nanosheets with thickness down to 10 nm. We find that the resistivity peak temperature T^* can be significant tuned by the nanosheet thickness. When the thickness is reduced from 160 nm to 40 nm, T^* reduces systematically from 145 K to 100 K. However, with thickness further reducing to 10 nm, T^* shifts up to higher temperature. From our analysis, the system takes a transition from topological semimetal with two types carriers to a single band with conventional hole carriers when the thickness is less than 40 nm. Furthermore, by tracking the thickness-dependence of carrier density, we find that the Fermi level shifts continuously downward from conduction band to the valence band with decreasing the thickness. Our experiment reveals a thickness-tuned transition of band topology in ZrTe_5 nanosheets which may be helpful for the understanding of the contrast observations in this material.

I. INTRODUCTION

Zirconium pentatelluride ZrTe_5 , a fascinating new three-dimensional (3D) Dirac semimetal, has recently attracted considerable attention. It hosts rich quantum phenomena related to the chiral fermions in its highly anisotropic three-dimensional Dirac bands.^{1,2,3} Comparing with other Dirac semimetals (e.g. Cd_3As_2 ^{4,5}, Na_3Bi ,⁶), its electronic structure presents extreme sensitivity to external perturbations such as magnetic fields, temperature, elastic tension or pressure.^{7,8,9,10} For example, recent angle-resolved photoemission spectroscopy (ARPES) experiment¹¹ shows that the temperature can induce a Lifshitz-type transition of electronic states from the hole band to electron band, leading to a resistance peak near the critical temperature T^* . The transport measurements on bulk ZrTe_5 also have demonstrated **clear** changes from hole-dominated states above T^* to electron dominated states below T^* .^{9,12} While the gapless topological Dirac semimetal phase has been **confirmed** in bulk ZrTe_5 ^{1,2,13,14,15} recent scanning tunneling microscopy (STM) experiments surprisingly detected a bulk band gap with topological edge states at the surface step edge which indicated that single layered ZrTe_5 might be a two-dimensional topological insulator that could host the quantum spin Hall effect (QSHE)^{16,17,18}. These contrast results indicate that the thickness, as an alternative way, may effectively tune the electronic structure in ZrTe_5 , though the mechanism has not been fully explored so far.

In this letter, we study the transport properties of ZrTe_5 nanosheets with thickness down to 10 nm. We find that the resistivity anomaly temperature T^* systematically shifts toward lower temperatures as the thickness **reduces** to 40 nm, indicating the suppression of the electron carriers in the Dirac band. When the nanosheet thickness is less than 40 nm, a broad resistive peak shows up at higher temperatures which moves up to room temperature with thickness further **reduced to 10 nm**. Both longitudinal resistivity and Hall resistivity measurements demonstrate that the resistance peak in

thinner nanosheets (< 40 nm) has a different origin from the bulk, where carriers in a secondary hole band **dominate** the transport. By tracking the carrier densities, a consecutive downward shifting of the Fermi level from conduction band to valence band is demonstrated as decreasing the thickness down to 10 nm, which reveals a thickness-tuned transition of the band topology in ZrTe₅ nanosheets.

II. EXPERIMENTAL TECHNIQUES

ZrTe₅ single crystals were grown via the iodine vapor transport method in a two-zone furnace as described in ref.19. **Stoichiometric amounts of elements Zr (99.99%) and Te (99.99%) lumps with 5 mg/cm³ iodine were sealed in evacuated quartz tube. The quartz tube was heated and kept at 590 °C for 2 days. Then the furnace gradient was kept between 590°C and 380°C for 14 days before turning off the furnace. To obtained high quantity ZrTe₅ crystals, the high purity and non-oxidation of Te lump is important.** The obtained crystals show a thin elongated rectangular shape with length up to centimeters. In this work, all the nanosheets were mechanically exfoliated from the bulk crystals, followed by directly transferring on Si/SiO₂ substrate. Hall bar devices were fabricated by standard electron-beam lithography followed by Au (80 nm)/Ti (10 nm) evaporation and lift-off process. Transport measurements were performed with physical properties measurement system (PPMS).

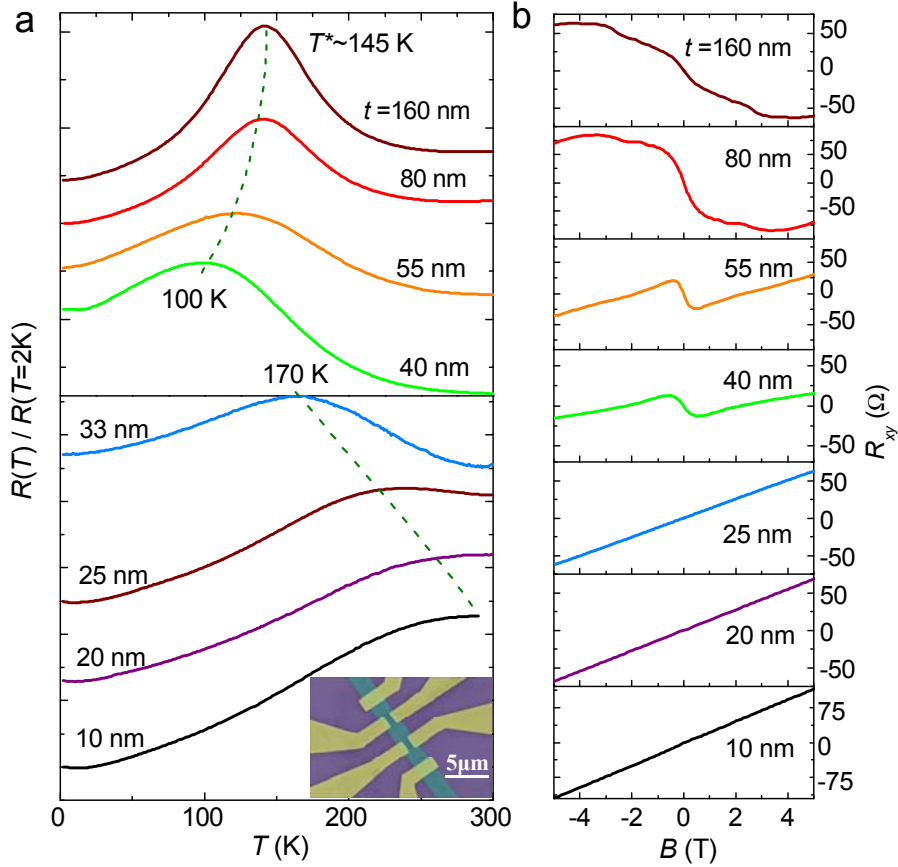


FIG. 1. (a) Normalized temperature dependence of longitudinal resistance ZrTe_5 nanosheets with different thickness. All curves are offset vertically for clarity. Inset: a SEM image of a Hall bar device used in the measurement. (b) Hall resistivity of the nanosheets with different thickness measured at $T = 2$ K.

III. RESULTS AND DISCUSSIONS

Figure 1a shows the normalized temperature dependence of resistance of ZrTe_5 nanosheets with different thickness. In the thick samples (e.g., $t = 160$ nm), the resistivity peak temperature T^* , defined from the peak position of the resistance-temperature ($R_{xx}-T$) curve, is about 145 K, which is consistent with the value in bulk single crystals.^{12,20} As the thickness is reduced to 40 nm, T^* decreases systematically to about 100 K. Strikingly, when the thickness is reduced to 33 nm, a broad

peak appears near 170 K which further shifts up to 300 K for the $t = 20$ nm sample. Figure 1b shows the Hall resistivity R_{xy} of these nanosheets **measured** at 2 K. For sample $t = 160$ nm, R_{xy} exhibits a typical multiband property with the electron band dominating the transport. With decreasing the thickness to 80 nm, the Hall coefficient, $R_H \propto R_{xy}/B$ with B the magnetic field, shows a sign reversal from negative in low field range to positive near 4 T. **Such a reversal is more pronounced for samples $t = 55$ nm and 40 nm. As a comparison, for samples $t = 25$ nm, 20 nm and 10 nm, R_{xy} shows a linear field dependence. This result indicates that the electron band is suppressed with thickness decrease and the hole carriers take over the transport properties in thin samples ($t < 40$ nm).** Hence, the role of decreasing thickness is same to the effect of lifting up temperature, *i.e.*, lowering down the Fermi level or shifts up the holes band. However, we note that the nanosheets with $t < 40$ nm present a metallic behavior, which is in contrast to the semiconductive hole band above T^* in thick samples. In other words, the hole carriers of the nanosheets $t < 40$ nm is probably not from the same hole band as indicated at high temperatures.

The longstanding question of the mechanism for the resistance peak at T^* is currently attributed to the upward shift of the Fermi level from the Dirac hole band to electron band with decreasing temperature,²¹ *i.e.*, the temperature-induced Lifshitz transition.¹¹ This can also be verified by the temperature-dependent Hall resistivity measurement for our thick nanosheets, *e.g.* $t = 55$ nm, as shown in Fig. 2a, where the Hall coefficient R_H near zero field shows a sign reversal from positive to negative near the peak temperature T^* (**~ 120 K**). To explore the electronic mechanism of the resistance anomaly in thin nanosheets ($t < 40$ nm), we have **measured** the Hall resistivity at different temperatures of sample $t = 33$ nm. As shown in Fig. 2b, the Hall resistivity shows a linear behavior with a positive slope, regardless of the temperature being below or above T^* (**~ 170 K**), which

provide evidence that hole carrier band dominates the transport in thinner nanosheets ($t < 40$ nm), and no transition of band topology occurs with temperature cooling through T^* . In other word, the origin of the broad resistance peak in thinner nanosheets cannot be attributed to the competition between electron and hole pockets which is different from the thick samples ($t > 40$ nm).

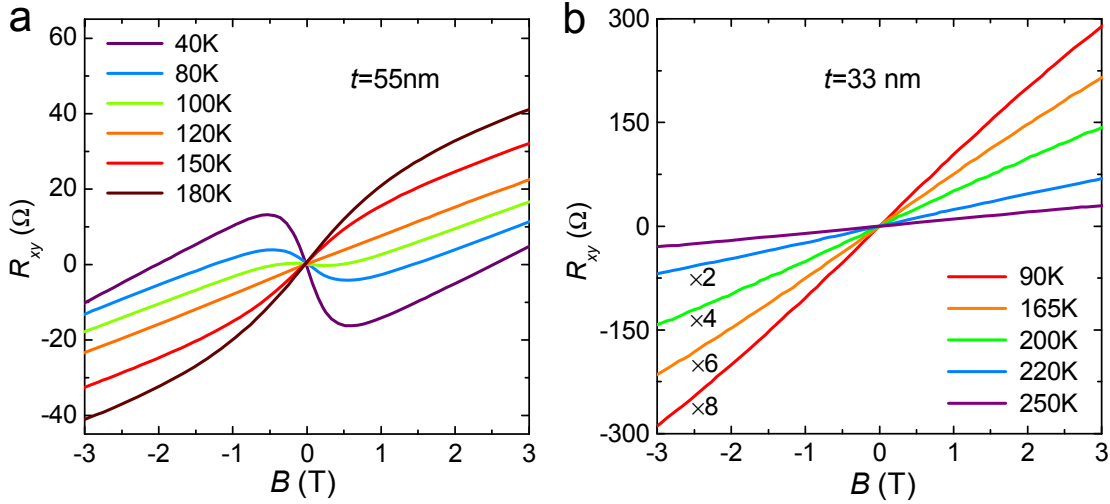


FIG. 2. The Hall resistivity under different temperature near T^* in ZrTe_5 nanosheets with thickness (a) $t=50$ nm and (b) $t=33$ nm.

To have a comprehensive insight on this conventional resistivity anomaly in thinner samples, we have tracked the temperature-dependence of carrier density and mobility in samples $t = 33$ nm and 25 nm, as shown in Fig.3. Since the Hall resistivity of both samples exhibits a linear behavior, we can evaluate the carrier density by the formula $n = 1/R_H e$, and the mobility μ by the relationship $\mu = \sigma/ne$, where e , σ , and n is the electron charge, zero field conductivity and carrier density, respectively. For both samples, the carrier density decreases sharply with temperature decrease while the mobility shows a opposite trend and increases gradually. Thus the broad resistivity peak is likely formed due to the opposite contributions of reducing charge carrier density n and increasing

mobility μ to the electrical resistivity. We note that similar upward shifting of the resistance anomaly temperature T^* has been observed in several work of ZrTe₅ nanosheets^{22,23}.

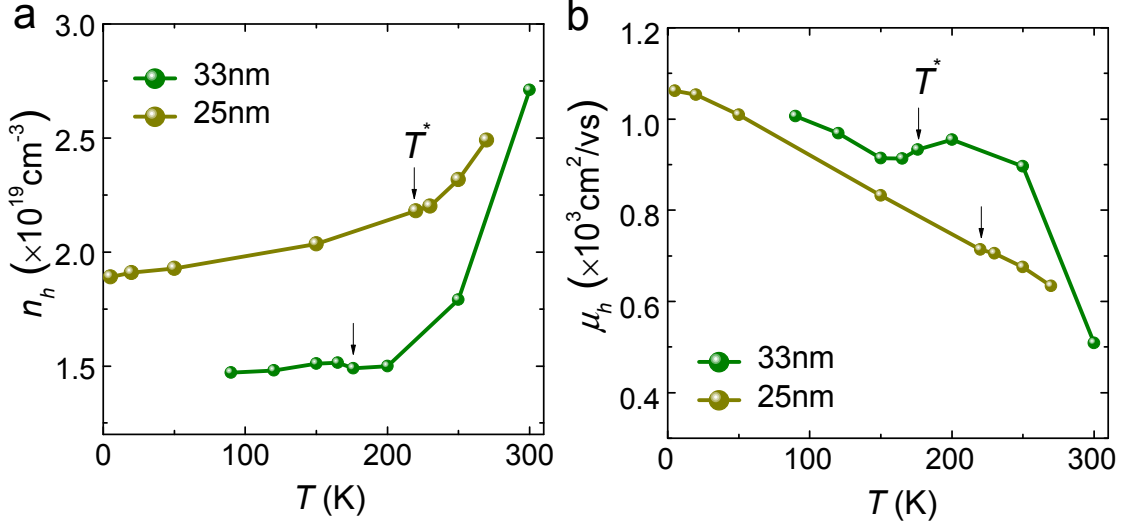


FIG. 3.

The temperature dependence of the carrier density (a) and mobility (b) in $t = 33$ nm and 25 nm thick samples. T^* is the resistivity anomaly temperature for different samples.

To full understand the thickness-tuned band topology, we have tracked the thickness-dependence of carrier density at $T = 2$ K. As shown in Fig. 4, for nanosheets with $t \geq 40$ nm, the two-band model was used to fit the Hall conductivity σ_{xy} ,

$$\sigma_{xy}(2\text{K}) = \left[n_1 \mu_1^2 \frac{1}{1+(\mu_1 B)^2} + n_2 \mu_2^2 \frac{1}{1+(\mu_2 B)^2} \right] eB, \quad (1)$$

where n_1 , n_2 are the carrier density in two different bands, and μ_1 and μ_2 are the mobility, correspondingly. Figure 4a shows the fitting result of Hall conductivity for samples $t \geq 40$ nm. The extracted carrier density as the function of thickness is shown in Fig. 4b. In thick nanosheets $t > 80$ nm, it contains a Dirac electron pocket with high mobility and a secondary electron band with low mobility. This result is consistent with recent ARPES experiments, where an off-centered secondary band is revealed, beside the Dirac band at the Brillouin Zone center.^{1,3,11} The carrier densities in both

electron pockets decrease with thickness reducing, hinting a downward shifting of the Fermi level. In samples $80 \text{ nm} \leq t \leq 40 \text{ nm}$, the carriers in the secondary band transforms from n -type to p -type. While in samples below 40 nm , only a single band with p -type carriers is revealed due to the linear behavior of Hall resistivity (shown in Fig.2 and 3). This p -type carrier density increases as decreasing the thickness down to 10 nm (shown in Fig.4b). These results demonstrate that, from $t = 160 \text{ nm}$ to 10 nm , the Fermi level shifts consecutively from conduction band down to the valence band which reveals a thickness-tuned band topology transition in ZrTe_5 nanosheets.

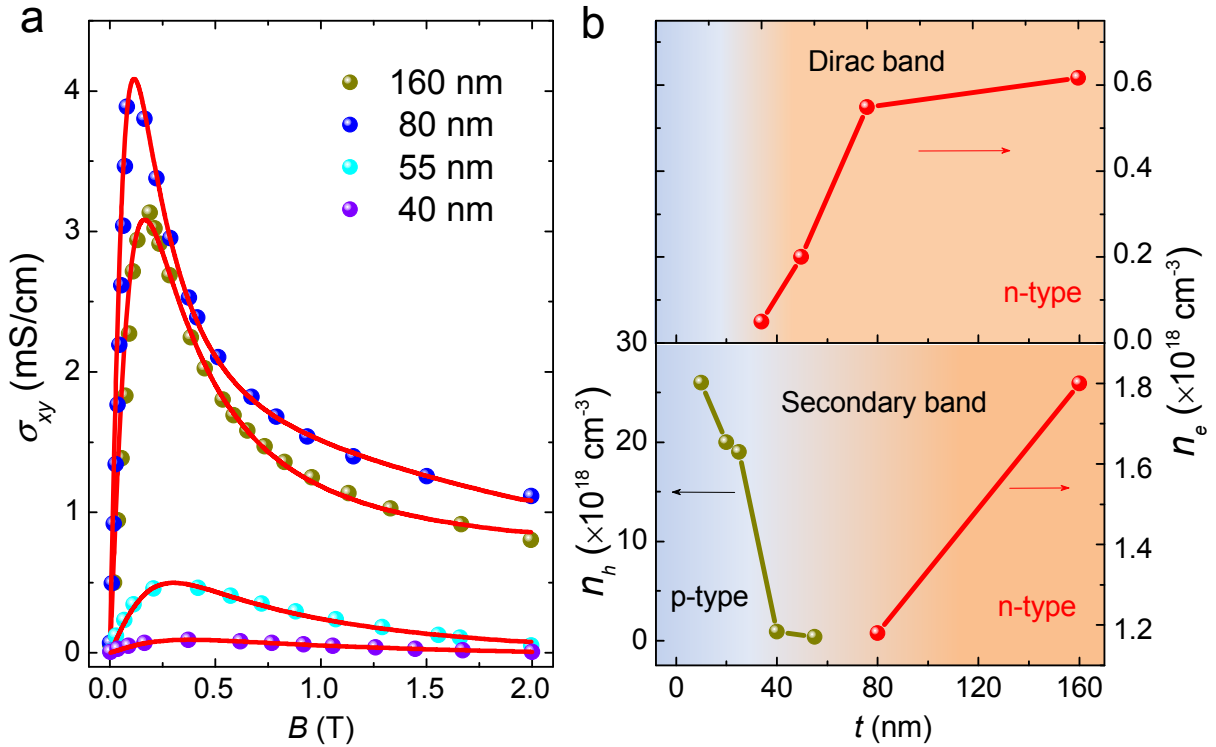


FIG. 4. (a) Two-band fitted Hall conductivity for nanosheets with thickness above 40 nm . The red curves are the fitting results while the solid circles are the experimental data. (b) The evolution of the carrier density as function of the thickness. n_e and n_h denote the electron and hole carrier density, respectively. Above 40 nm , the band structure consists of two electron pockets, a 3D Dirac band (with low carrier density and high mobility) and a secondary band. Below 40 nm , only a single hole band is revealed.

To gain deeper understanding of the electronic nature of ZrTe₅ nanosheets, we have explored the longitudinal magnetoresistance (MR) of samples with different thicknesses, as shown in Fig. 5. When fitting the MR curve by a formula of $R \propto B^\alpha$, with α the fitting parameter, it is clearly that the MR presents a quasi-linear behavior with an exponent α close to 1 in thick nanosheets ($t \geq 80$ nm). Such a linear MR has been widely seen in topological insulator and topological semimetal with linear energy dispersion^{24,25,26}. For samples $t = 55$ and 40 nm, the MR follows a \sqrt{B} type behavior with $\alpha \sim 0.5$, indicating the weak antilocalization (WAL) effect in a 3D topological semimetal.²⁷ In contrast, the MR exhibits a simple quasi-quadratic behavior with $\alpha \sim 1.6$ when the thickness is less than 40 nm. When tracking the MR behavior in very low field region, we found that the MR exhibits a quasi-quadratic behavior with $\alpha \sim 2$ for thick nanosheets ($t \geq 40$ nm), as shown in the log-log plot of the MR curves in Fig.5b. While for nanosheets $t < 40$ nm, the low field MR shows a \sqrt{B} tendency with $\alpha \sim 0.5$. As discussed above, the Fermi level shifts downward consecutively to the Dirac point with decreasing thickness. Thus, it can be inferred that the \sqrt{B} -type MR induced by WAL effect in the presence of the weak intervalley scattering will surpass the B^2 -type MR when decreasing the thickness below 40 nm. Unfortunately, we cannot determine whether there is a band gap or not in the Dirac band in the thinner nanosheets since no SdH quantum oscillations were observed in our studied field range. The fact that the nanosheets with $t < 40$ nm show excellent metallic behavior with hole carriers demonstrates that the secondary hole band dominate the transport and most likely have a conventional nature. This is qualitatively consistent with recent magnetoinfrared spectroscopy experiments in thin ZrTe₅ nanoflakes, where a zero magnetic field optical absorption with a photon energy 10 meV hints the existence of 3D massive Dirac Fermions for thin ZrTe₅ nanosheets²⁸.

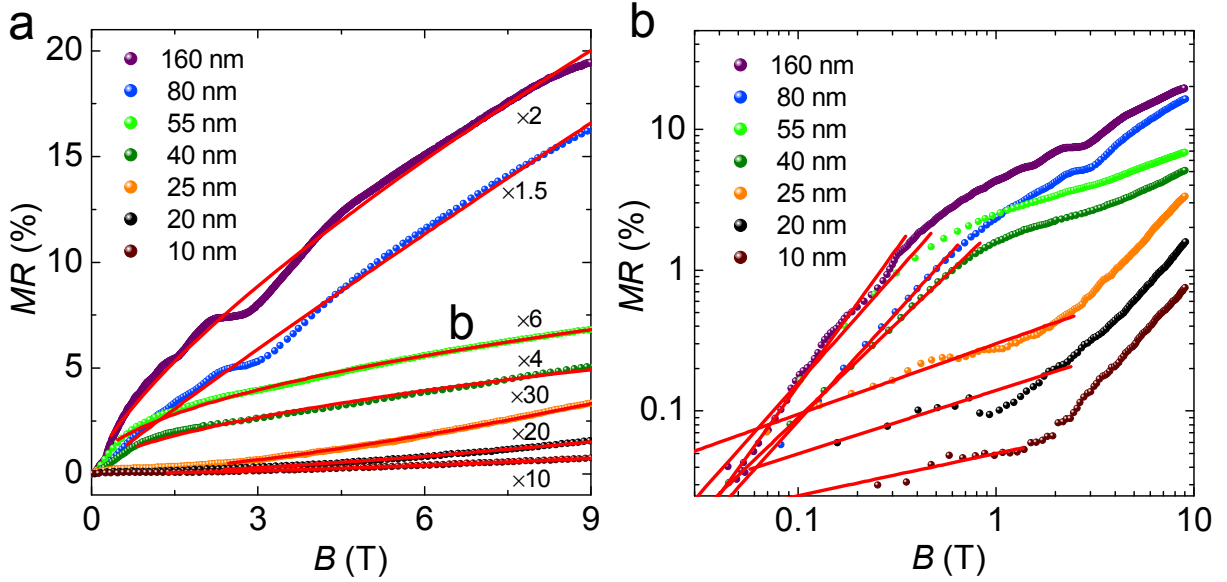


FIG. 5. (a) The magnetoresistance (MR) curves of ZrTe_5 nanosheets with different thickness measured at $T = 2$ K. (b) The log-log plot of the MR curves. The red curves are the fitting curves with a formula of $R \propto B^\alpha$.

IV. CONCLUSION

In conclusion, we have systematically studied the transport properties of 3D Dirac semimetal ZrTe_5 nanosheets with different thickness. We found that the resistivity anomaly temperature evolves non-monotonically with decreasing the thickness. Detailed Hall measurements suggest that the anomalous resistivity with peak in thinner ZrTe_5 nanosheets ($t < 40$ nm) stems from a totally different mechanism to that in thick samples ($t \geq 40$ nm). Further analysis of the carrier density demonstrates that the Fermi level shifts consecutively from conduction band to valence band with decreasing thickness. Our experiments provide a comprehensive insight on the thickness-dependent electronic structures in 3D Dirac semimetal ZrTe_5 , which would be helpful for the understanding of this complex layered material and further study on nanodevices.

Acknowledgments

This work was supported by the Natural Science Foundation of China (Grant No. 11574320, No. 11174294, No.11374302, No.11204312, No. 1147289, No.U1432251), and the National Key Research and Development Program of China No.2016YFA0401003, the program of Users with Excellence, the Hefei Science Center of CAS, the CAS/SAFEA international partnership program for creative research teams of China, and National Science Foundation through grants No. DMR-1004545 and No.DMR-1442366.

Reference

-
- ¹ Q. Li, D. E. Kharzeev, C. Zhang, Y. Huang, I. Pletikoscic, A. V. Fedorov, R. D. Zhong, J. A. Schneeloch, G. D. Gu, and T. Valla, *Nat. Phys.* **12**, 550 (2016).
 - ² G. Zheng, J. Lu, X. Zhu, W. Ning, Y. Han, H. Zhang, J. Zhang, C. Xi, J. Yang, H. Du, K. Yang, Y. Zhang, and M. Tian, *Phys. Rev. B* **93**, 115414 (2016).
 - ³ L. Shen, M. Wang, S. Sun, J. Jiang, X. Xu, T. Zhang, Q. Zhang, Y. Lv, S. Yao, Y. Chen, M. Lu, Y. Chen, C. Felser, B. Yan, Z. Liu, L. Yang, and Y. Chen, *J. Electron. Spectrosc. Relat. Phenom.* (in press)
 - ⁴ Z. Liu, J. Jiang, B. Zhou, Z. Wang, Y. Zhang, H. Weng, D. Prabhakaran, S.-K. Mo, H. Peng, P. Duding, T. Kim, M. Hoesch, Z. Fang, X. Dai, Z. Shen, D. Feng, Z. Hussain, Y. Chen, *Nat. Mater.* **13**, 677 (2014).
 - ⁵ M. Neupane, S. Xu, R. Sankar, N. Alidoust, G. Bian, C. Liu, L. Belopolski, T.-R. Chang, H.-T. Jeng, H. Lin, A. Bansil, F. Chou, and M. Z. Hasan, *Nat. Commun.* **5**, 3786 (2014).
 - ⁶ Z. Liu, B. Zhou, Y. Zhang, Z. Wang, H. Weng, D. Prabhakaran, S.-K. Mo, Z. Shen, Z. Fang, X. Dai, Z. Hussain, and Y. Chen, *Science* **343**, 864 (2014).
 - ⁷ E. P. Stillwell, A. C. Ehrlich, G. N. Kamm, and D. J. Gillespie, *Phys. Rev. B* **39**, 1626 (1989).
 - ⁸ Y. Zhou, J. Wu, W. Ning, N. Li, Y. Du, X. Chen, R. Zhang, Z. Chi, X. Wang, X. Zhu, P. Lu, C. Ji, X. Wan, Z.

-
- Yang, J. Sun, W. Yang, M. Tian, Y. Zhang, and H.-K. Mao, *Proc. Natl. Acad. Sci. U.S.A.* **113**, 2904 (2016).
- ⁹ Y. Liu, X. Yuan, C. Zhang, Z. Jin, A. Narayan, C. Luo, Z. Chen, L. Yang, J. Zou, X. Wu, S. Sanvito, Z. Xia, L. Li, Z. Wang, and F. Xiu, *Nat. Commun.* **7**, 12516 (2016).
- ¹⁰ G. Zheng, X. Zhu, J. Lu, W. Ning, H. Zhang, W. Gao, Y. Han, J. Yang, H. Du, K. Yang, Y. Zhang, and M. Tian, *arXiv:1607.05384*.
- ¹¹ Y. Zhang, C. Wang, L. Yu, G. Liu, A. Liang, J. Huang, S. Nie, Y. Zhang, B. Shen, J. Liu, H. Weng, *et al.*, *arXiv:1602.03576*.
- ¹² D. N. Mellroy, S. Moore, D. Zhang, J. Wharton, B. Kempton, R. Littleton, M. Wilson, T. M. Tritt, and C. G. Olson, *J. Phys. Condens. Matter.* **16**, L359 (2004).
- ¹³ G. Manzoni, A. Crepaldi, G. Autès, A. Sterz, F. Cilento, A. Akrap, I. Vobornik, L. Gragnaniello, Ph. Bugnon, M. Fonin, H. Berger, M. Zacchigna, O.V. Yazyev, and F. Parmigiani. *J. Electron. Spectrosc. Relat. Phenom.* (in press)
- ¹⁴ Y. R. Chen, Z. G. Chen, X.-Y. Song, J. A. Schneeloch, G. D. Gu, F. Wang, and N. L. Wang, *Phys. Rev. Lett.* **115**, 176404 (2015).
- ¹⁵ Y. R. Chen, S. Zhang, J. A. Schneeloch, C. Zhang, Q. Li, G. D. Gu, and N. L. Wang, *Phys. Rev. B* **92**, 075107 (2015).
- ¹⁶ H. Weng, X. Dai, and Z. Fang, *Phys. Rev. X* **4**, 011002 (2014).
- ¹⁷ R. Wu, J. Z. Ma, S. M. Nie, L. Zhao, X. Huang, J. X. Yin, B. B. Fu, P. Richard, G. F. Chen, Z. Fang, X. Dai, H. M. Weng, T. Qian, H. Ding, and S. H. Pan, *Phys. Rev. X* **6**, 021017 (2016).
- ¹⁸ X. B. Li, W. K. Huang, Y. Y. Lv, K. W. Zhang, C. L. Yang, B. B. Zhang, Y. B. Chen, S. H. Yao, J. Zhou, M. H. Lu, L. Sheng, S. C. Li, J. F. Jia, Q. K. Xue, Y. F. Chen, and D. Y. Xing, *Phys. Rev. Lett.* **116**, 176803 (2016).
- ¹⁹ G. N. Kamm, D. J. Gillespie, A. C. Ehrlich, T. J. Wieting, and F. Levy, *Phys. Rev. B* **31**, 7617 (1985).
- ²⁰ T. M. Tritt, N. D. Lowhorn, R. T. Littleton, A. Pope, C. R. Feger, and J. W. Kolis, *Phys. Rev. B* **60**, 7816 (1999).
- ²¹ G. Manzoni, A. Sterzi, A. Crepaldi, M. Diego, F. Cilento, M. Zacchigna, P. Bugnon, H. Berger, A. Magrez,

-
- M. Grioni, and F. Parmigiani, *Phys. Rev. Lett.* **115**, 207402 (2015).
- ²² J. Niu, J. Wang, Z. He, C. Zhang, X. Li, T. Cai, X. Ma, S. Jia, D. Yu, and X. Wu, *Phys. Rev. B.* **95**, 035420 (2017)..
- ²³ G. Qiu, Y. Du, A. Charnas, H. Zhou, S. Jin, Z. Luo, D. Y. Zemlyanov, X. Xu, G. J. Cheng, and P. D. Ye, *Nano Lett.* **16**, 7364 (2016)
- ²⁴ A. Narayanan, M. D. Watson, S. F. Blake, N. Bruyant, L. Drigo, Y. L. Chen, D. Prabhakaran, B. Yan, C. Felser, T. Kong, P. C. Canfield, and A. I. Coldea, *Phys. Rev. Lett.* **114**, 117201 (2015).
- ²⁵ X. Wang, Y. Du, S. Dou, and C. Zhang, *Phys. Rev. Lett.* **108**, 266806 (2012).
- ²⁶ J. Feng, Y. Pang, D. Wu, Z. Wang, H. Weng, J. Li, X. Dai, Z. Fang, Y. Shi, and L. Lu, *Phys. Rev. B* **92**, 081306(R) (2015).
- ²⁷ H. Lu, and S.-Q. Shen, *Phys. Rev. B* **92**, 035203 (2015).
- ²⁸ Z. G. Chen, R. Y. Chen, R. D. Zhong, J. Schneeloch, C. Zhang, Y. Huang, F. M. Qu, R. Yu, Q. Li, G. D. Gu, N. L. Wang, *Proc. Natl. Acad. Sci.* **114**, 816-821 (2017).